Social Behavior, Mixing, and the Evolution of Schooling

Glenn Flierl
Notes by Kiori Obuse and Emma Boland (née Thompson)

May 11, 2011

1 Introduction

Swimming organisms adjust their behavior in response to environmental conditions and form structures such as patches, swarms, and schools. Disadvantages of these tendencies include tougher competition for food, the attraction of predators; some hydrodynamic disadvantages – turbulent wakes disrupt movement, and more energy is required to swim, etc. There are several advantages however, such as enhanced reproduction, predator avoidance, and the easier search for prey; some hydrodynamic advantages – extra turbulence brings higher encounter rates, and coordinated swimming. Here, we study a model for such organisms' behavior.

2 Lagrangian Dynamics

In order to consider the model mentioned above, we start with the Lagrangian dynamics of an individual or molecule of fluid. The stochastic differential equations for the position $\mathbf{X}$ and velocity $\mathbf{U}$ are

$$dX_i = U_i dt, \tag{1}$$

$$dU_i = A_i dt + \beta_{ij} dW_j, \tag{2}$$

where $\mathbf{A}$ is the acceleration produced by deterministic, or large-scale, forces, $\beta_{ij} dW_j$ is the random acceleration, with the random increment dW_j satisfying $\langle dW_i \rangle = 0$ and $\langle dW_i \; dW_j \rangle = \delta_{ij} dt$, and β_{ij} will be a diagonal matrix. The equations (1) and (2) also hold for continuous $\mathbf{X}$ and discrete $\mathbf{U}$. As an example, consider a drag law for the acceleration

$$\mathbf{A} = -r(\mathbf{U} - \mathbf{u}), \tag{3}$$

with $\mathbf{u}$ being the water velocity and $\beta_{ij} = \beta \delta_{ij}$. Then the dispersion is determined by β and r; from the equations, by assuming that the statistics become time-independent for large t, $\langle U_i(t) \rangle = \langle U_i(t + dt) \rangle$ in the long-time limit or solving the equations (1) and (2) by utilizing Ito's lemma (see, for example, [2]), we can show that

$$\langle U_i \rangle \to u_i, \tag{4}$$

$$\langle (U_i - u_i)(U_j - u_j) \rangle \to \frac{\beta^2}{2r} \delta_{ij}, \tag{5}$$

$$\langle X_i(t) X_j(t) \rangle \to \langle X_i(0) X_j(0) \rangle + \frac{\beta^2}{r^2} \delta_{ij} t. \tag{6}$$

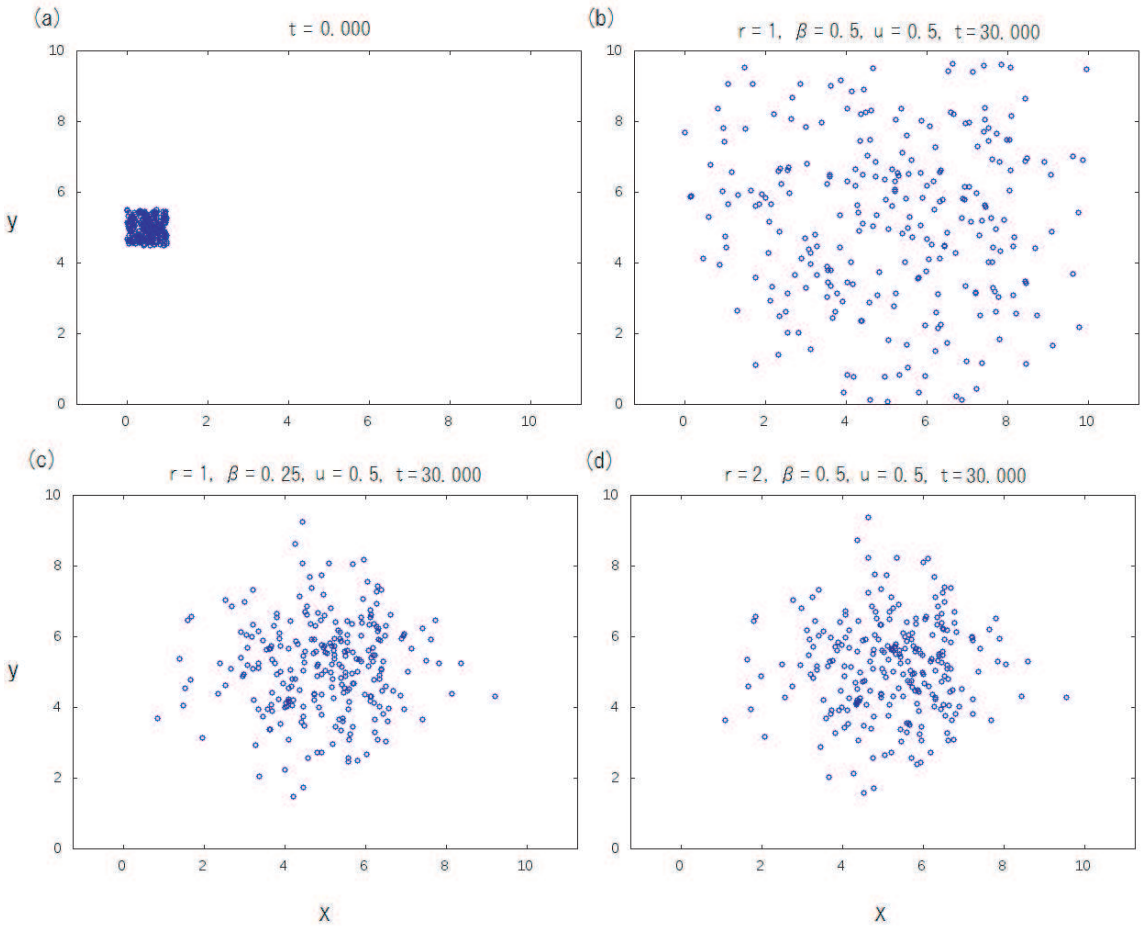

Figure 1: Distributions produced by numerical simulation of Lagrangian particles from equations (1,2), showing (a) the initial conditions for all cases, (b) $r = 1, \beta = 0.5, u = 0.5, t = 30$, (c) $r = 1, \beta = 0.25, u = 0.5, t = 30$, (d) $r = 2, \beta = 0.5, u = 0.5, t = 30$.

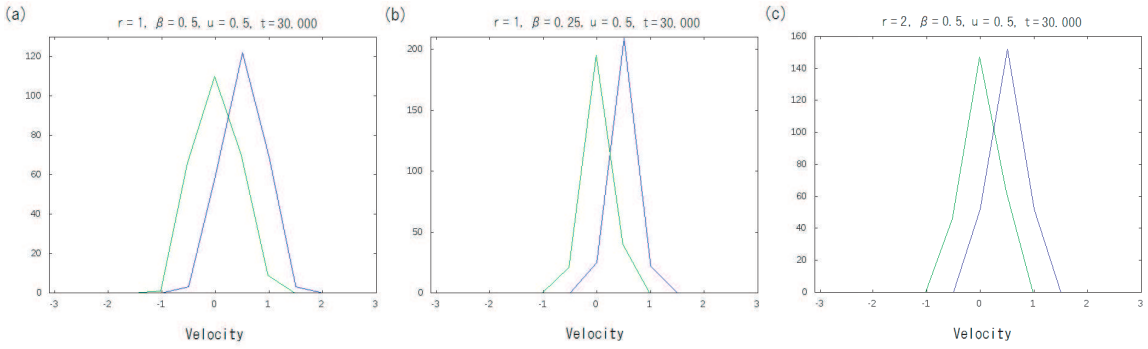

Figure 2: Histogram of velocities from numerical simulations of Lagrangian particles with the parameters (a) $r = 1, \beta = 0.5, u = 0.5, t = 30$ (b) $r = 1, \beta = 0.5, u = 0.25, t = 300$ (c) $r = 2, \beta = 0.5, u = 0.5, t = 30$. The blue and the green lines in each panel represent the velocities in the x- and y-directions, respectively.

As diffusion coefficient κ is $\kappa \equiv \langle dX_i dX_j \rangle / (2dt)$, the latter corresponding to a diffusivity of $\kappa = \beta^2/2r^2$, which means that the area grows like $4\kappa t$ and the velocity variance is $r\kappa$.

Figure 1 contains snapshots of the distribution of particles for different combinations of the parameters r and β. We can see that the area occupied by the particles grows more for larger β (see Fig.1(b) and (c)) and smaller r(see Fig.1 (b) and (d)). This can also be confirmed by the probability density functions (not normalized to one) of the x- and y-velocities shown in Fig.2.

3 Grouping Mechanisms

To consider a variety of motions, we use the form

$$dX_i = U_i dt,$$

$$dU_i = -r(U_i - u_i - V_i)dt + \beta_{ij} dW_j. \tag{7}$$

Here, $\mathbf{V}$ denotes the preferred swimming velocity, swimming towards the surface for example. Now we distinguish between various behaviors of swimming organisms. The properties described below maybe used individually or together, depending upon the organisms considered.

- taxis: $\mathbf{V}$ depends on gradient of cue field $\nabla C(\mathbf{x}, t)$ (Fig.3), where cue $C(\mathbf{x}, t)$ may be environmental (food, light, depth, etc.) or social (positions of neighbors, etc.). This describes a large-scale preferred velocity that the group tends to.

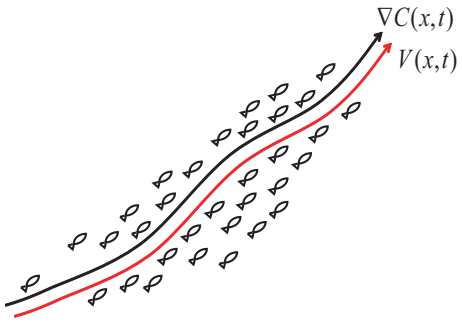

Figure 3: Representation of taxis.

Here, we define taxis as a preference for moving up the gradient of the cue field,

$$\mathbf{V} = \alpha \nabla C(\mathbf{x}).$$

As an example, we consider

$$C = C_0 \left[1 - \cos(kx)\right] / 2 \tag{8}$$

so that $\mathbf{V} = V_0 \sin(kx)\hat{\mathbf{x}}$ and $\mathbf{A} = -r\left[\mathbf{U} - \mathbf{u} - V_0 \sin(kx)\hat{\mathbf{x}}\right]$. Figures 4 and 5 show the distribution and the PDF (not normalized to one) of the organisms taken from numerical

simulations, respectively. Taxis on a spatially and temporally fixed cue field has its center of aggregation where $\nabla \cdot \mathbf{V}_{pref}$ (or $\nabla^2 C$) is most negative when there is no advection (see Fig.4 (b)), and the advection can shift this downstream (see Fig.4 (b)-(d)), which decreases the strength of the aggregation as a result (see Fig.4 (b), (c), and (d)). We can also see that the diffusion coefficient $\kappa = \beta^2/2r^2$ controls the width of the aggregation (Figs.4, 5).

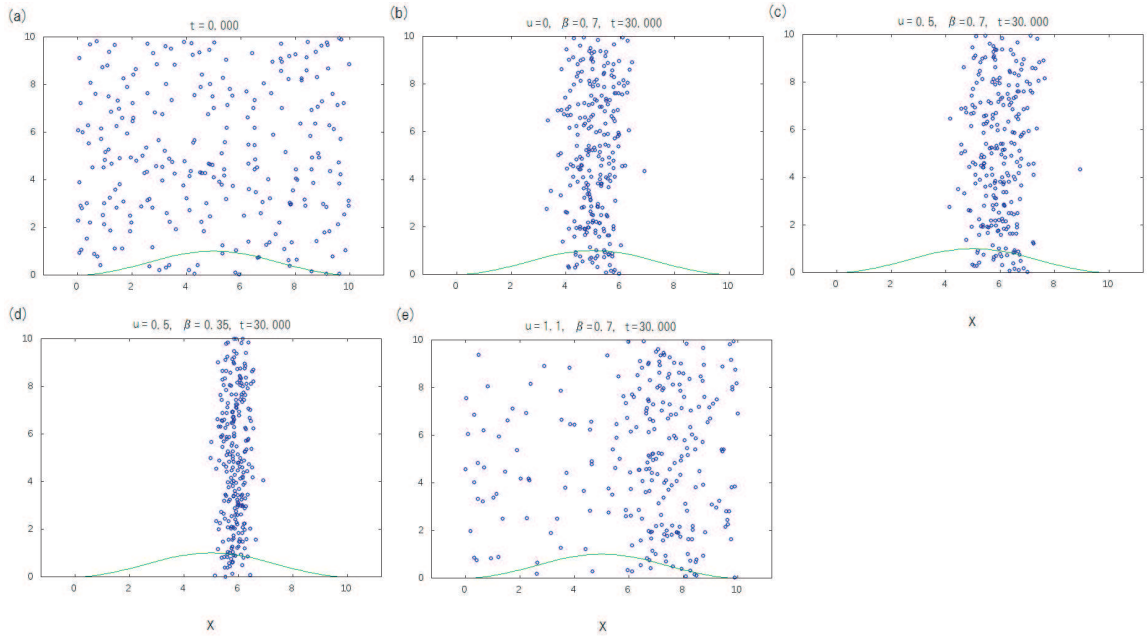

Figure 4: Taxis: Numerical simulation results of the example described in Section 3 showing organism distribution (blue dots) and the profile of C (green line) with (a) the initial conditions for all cases, (b) $u = 0, \beta = 0.7, t = 30$, (c) $u = 0.5, \beta = 0.7, t = 30$, (d) $u = 0.5, \beta = 0.35, t = 30$, (e) $u = 1.1, \beta = 0.7, t = 30$.

We then define *social* taxis as grouping when the cue field is defined in terms of the positions of other organisms;

$$C(\mathbf{X}) = \sum_{\mathbf{X}'} \left[\frac{1}{4} |\mathbf{X}' - \mathbf{X}|^4 - \frac{1}{2} |\mathbf{X}' - \mathbf{X}|^2 \right], \quad |\mathbf{X}' - \mathbf{X}| < 1, \tag{9}$$

so that the ∇C can be expressed as $\nabla C = (\mathbf{X} - \mathbf{X}')w(|(\mathbf{X} - \mathbf{X}')|)$ with weight function w having the profile shown in Fig.6. Using this form of social taxis, the temporal variation of the aggregation of the considered organisms depends upon the displacement of each set of two organisms, *i.e.* $|\mathbf{X}' - \mathbf{X}|$, and so groups close to each other merge as time progresses as shown in Fig.7 (note the groups in red circles).

- kinesis: β depends on the cue field:

$$\beta = \beta(C). \tag{10}$$

  This describes an individual's tendency to move randomly, when they, for example, find some food close to them (Fig.8), and is a more primitive response in which the random accelerations increase or decrease depending on the cue field.

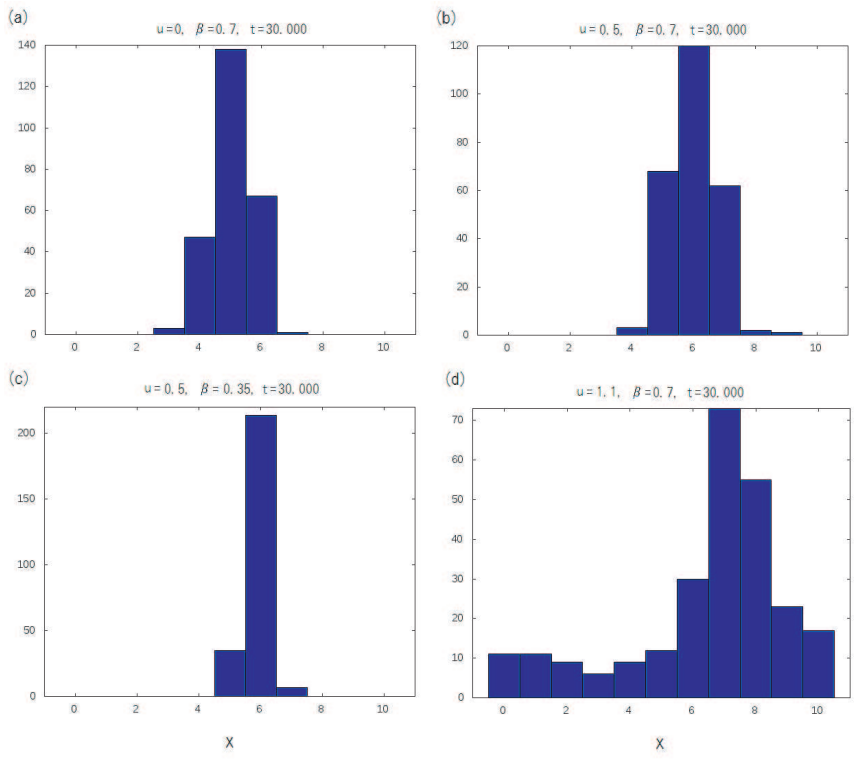

Figure 5: Taxis: Histograms from numerical simulations of organism distribution in the x-direction for (a) $u = 0, \beta = 0.7, t = 30$, (b) $u = 0.5, \beta = 0.7, t = 30$, (c) $u = 0.5, \beta = 0.35, t = 30$, (d) $u = 1.1, \beta = 0.7, t = 30$.

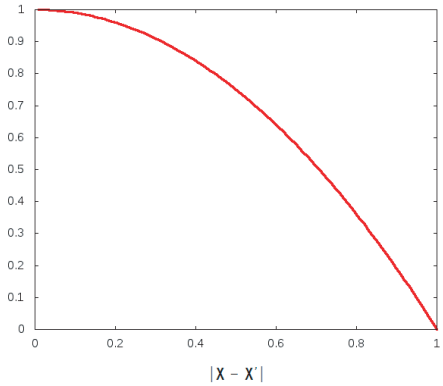

Figure 6: An example of the weight function $w(|\mathbf{X}' - \mathbf{X}|)$ used in social taxis. Here, $w(x) = (|x|^3 - |x|)/x$.

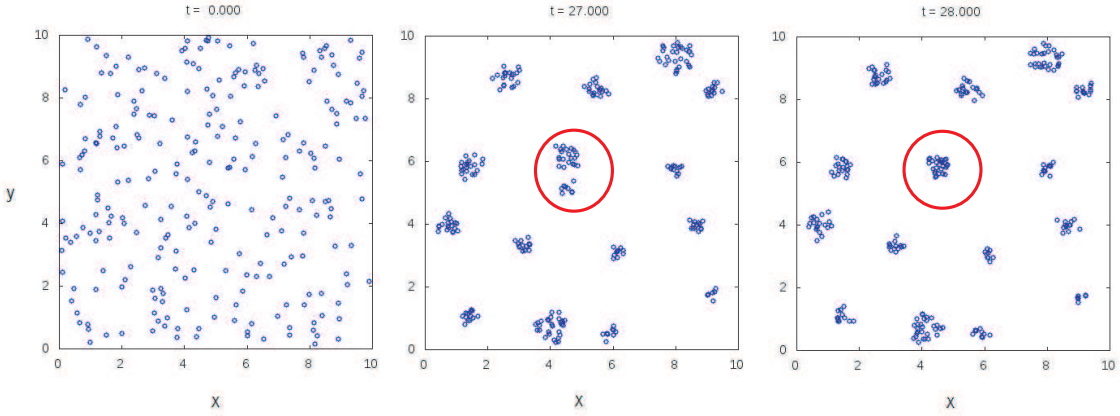

Figure 7: Social Taxis: The temporal variation of organism distributions from numerical simulations. From left to right, the panels show the organism distribution at times $t = 0, t = 27$, and $t = 28$.

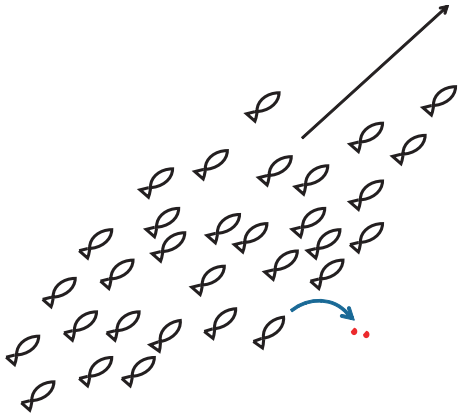

Figure 8: Representation of kinesis.

Let $\beta = \beta_0 - \beta_1 C/C_0$, for example, and consider C given by (8) again. Figures 9 and 10 show example distributions of organisms from numerical simulations. Kinesis can produce aggregation since β decreases as C increases, which means dU/dt decreases as C increases. The groups tend to be looser however, depending upon β_{max}/β_{min}, and $\mathbf{u}$ as mentioned before.

As another example of kinesis, we assume that the organisms turn more frequently and have smaller mean free path in the presence of many neighbors. Now we consider β in the form $\beta \propto \exp(-C/C_0)$, and write *social* kinesis as

$$C(\mathbf{X}) = \sum_{\mathbf{X}'} \left[1 - |\mathbf{X} - \mathbf{X}'|^2\right], \quad |\mathbf{X} - \mathbf{X}'| < 1.$$

This does not include the fourth order term as in (9), since social kinesis appears in β as a non-derivative form. The possible situations that can be produced are some random turning, more random turning, and the avoidance of others as shown in Fig.11.

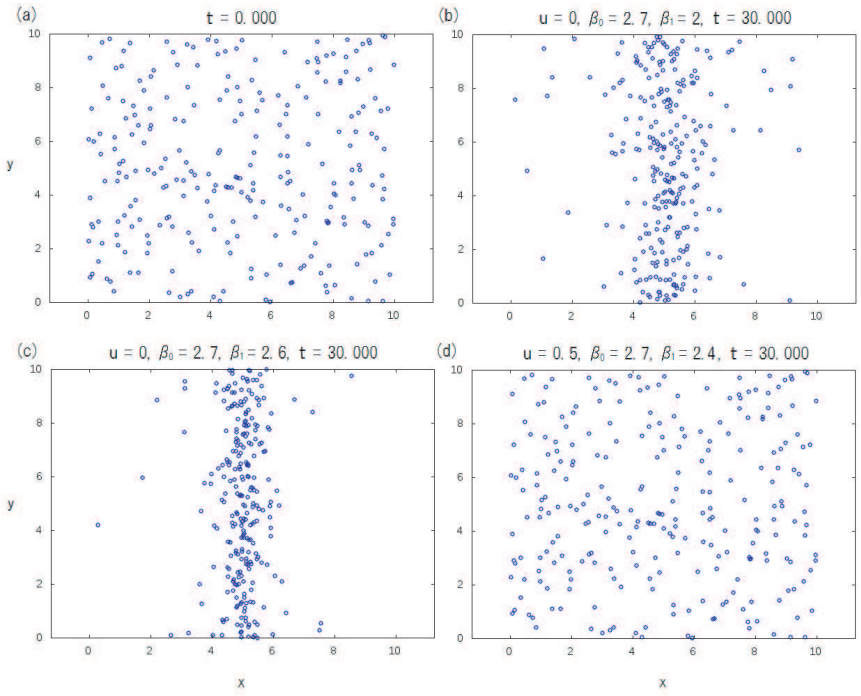

Figure 9: Kinesis: Distributions of organisms from numerical simulations with (a) initial time for all cases, (b) $u = 0, \beta_0 = 2.7, \beta_1 = 2.0, t = 30$, (c) $u = 0, \beta_0 = 2.7, \beta_1 = 2.6, t = 30$, (d) $u = 0.5, \beta_0 = 2.7, \beta_1 = 2.4, t = 30$.

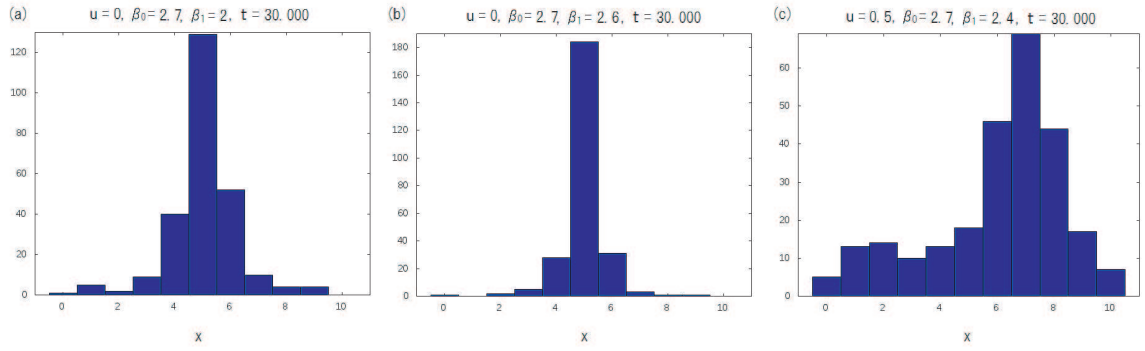

Figure 10: Kinesis: Histograms of organism distributions in the x-direction from numerical simulations for (a) $u = 0, \beta_0 = 2.7, \beta_1 = 2.0, t = 30$, (b) $u = 0, \beta_0 = 2.7, \beta_1 = 2.6, t = 30$, (c) $u = 0.5, \beta_0 = 2.7, \beta_1 = 2.4, t = 30$.

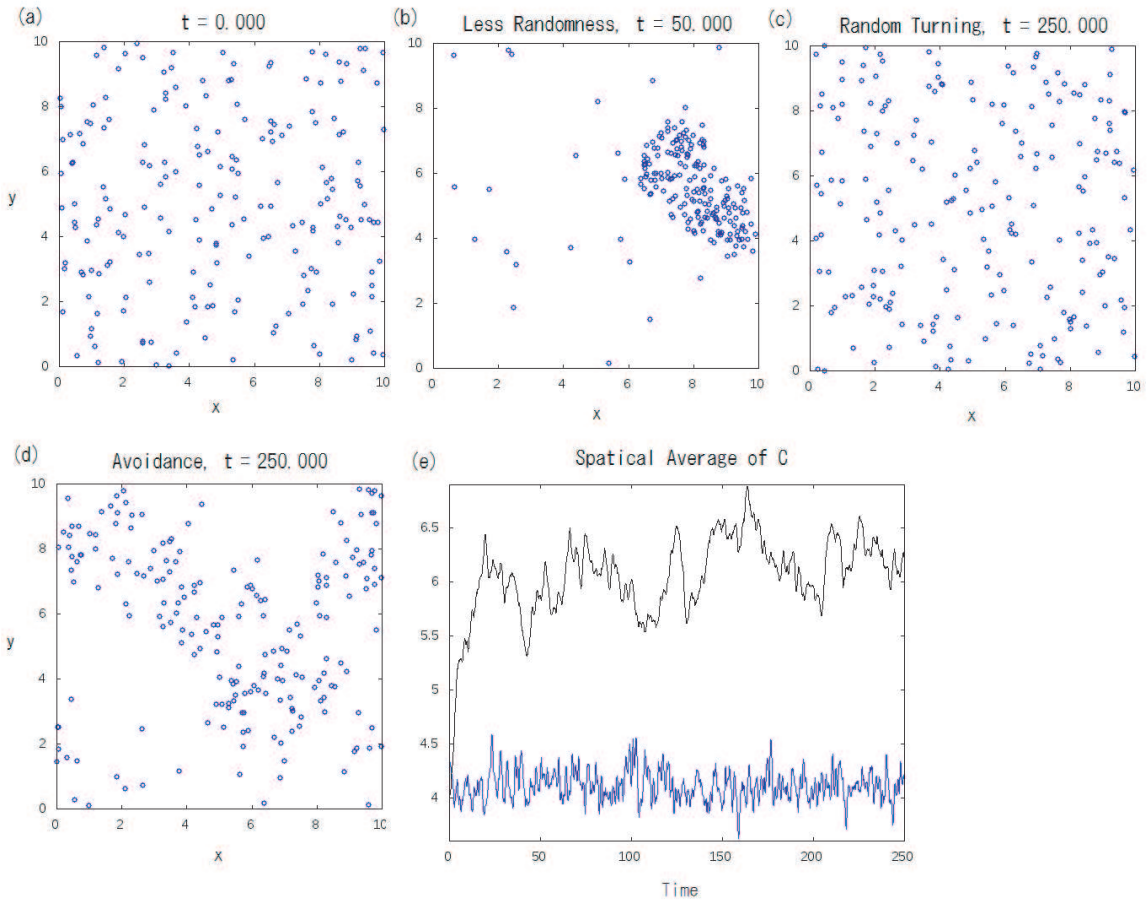

Figure 11: Social kinesis. (a)-(d) Distributions of organisms from numerical simulations showing (a) the initial distribution for all cases, distributions after the time shown in the cases (b) with some random turning, (c) more frequent random turning, and (d) organisms avoiding neighbors; and (e) the temporal variation of spatial average of C for panels (c) (blue) and (d) (black).

In the case that organisms turn randomly occasionally, the system ends up with a large group of organisms (Fig.11(b)), whilst the other two cases end up with much looser groups (Fig.11(c) and (d)). Comparing the cases of turning randomly and avoidance, the avoidance case shows stronger grouping, since the small mean free path interferes with the avoiding behaviour. This can also be verified by the temporal variation of the spatial average of the social kinesis C, which measures the strength of the grouping; the avoidance case shows a much larger value of average C than that of the case with frequent random turning(Fig.11(e)).

- Schooling: $\mathbf{V}$ depends on neighbor's $\mathbf{U}$ with $|\mathbf{V}|$ having a fixed value (Fig.12): $\mathbf{V} = \mathbf{V}(\mathbf{U}_{\text{neighbors}})$. This describes the behavior of the organisms that tend to swim similarly to their neighbors.

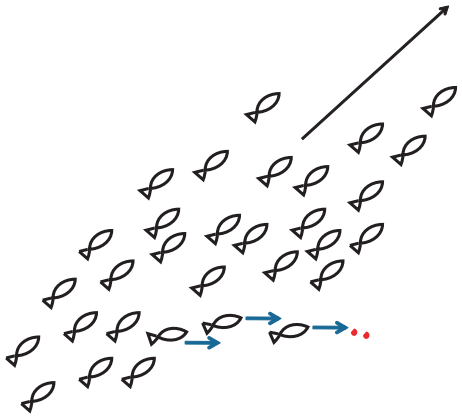

Figure 12: Representation of schooling.

The preferred direction of the swimming organisms results from a combination of attraction and alignment tendencies, and so schooling can be represented as

$$\mathbf{V} = V_0 \mathbf{V}_1 / |\mathbf{V}_1|,$$

$$\mathbf{V}_1 = \alpha \sum_{\mathbf{X}'} (\mathbf{X}' - \mathbf{X}) w(|\mathbf{X}' - \mathbf{X}|) + \sum_{\mathbf{X}'} \mathbf{U}' w(|\mathbf{X}' - \mathbf{X}|).$$

The first term represents attraction to neighbors. α controls the strength of the attraction; larger α gives stronger schooling as seen in Figure 13 which shows the temporal variation of organism distributions from numerical simulations for different α. Paying attention to the groups surrounded by circles, we notice that the case $\alpha = 0.3$ shows weak schooling and the groups tend to break apart easily, whilst the case $\alpha = 0.7$ shows much stronger schooling. The second term represents the tendency of organisms to align their swimming with their neighbors. The distance between two organisms at which alignment becomes effective tends to be smaller than that for attraction, as shown in Fig.14. Here, the choice of the weighting function w affects the internal structure of self-organized groups.

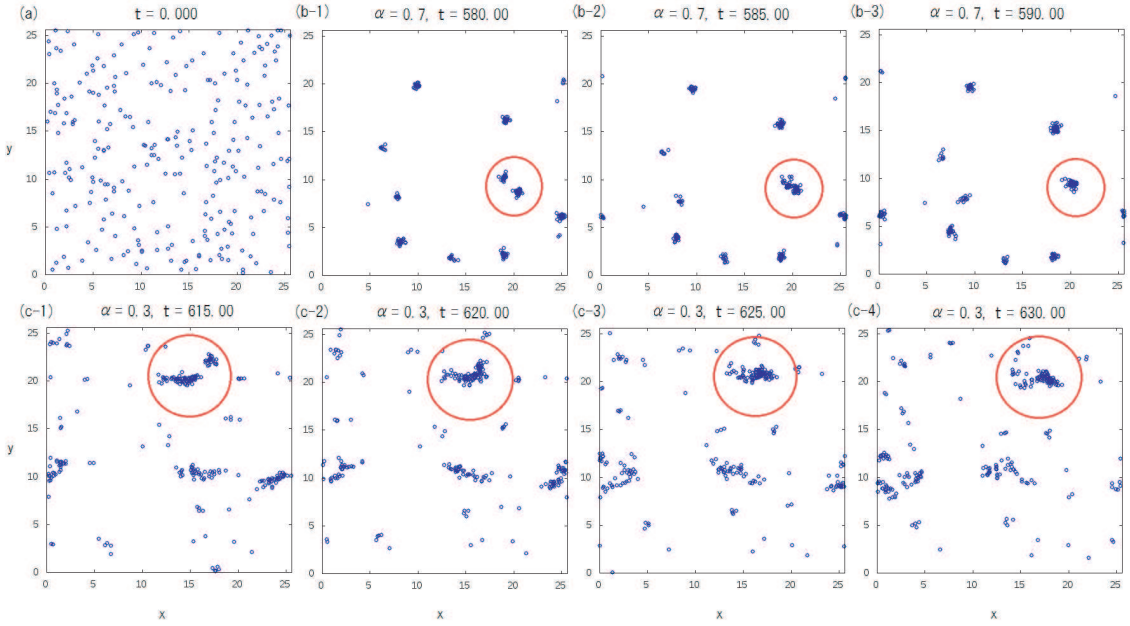

Figure 13: Schooling: Snapshots of organism distributions from numerical simulations. (a) the initial condition for all cases, (b-1) $\alpha = 0.7, t = 580$, (b-2) $\alpha = 0.7, t = 585$, (b-3) $\alpha = 0.7, t = 590$, (c-1) $\alpha = 0.3, t = 615$, (c-2) $\alpha = 0.3, t = 620$, (c-3) $\alpha = 0.3, t = 625$, (c-4) $\alpha = 0.3, t = 630$.

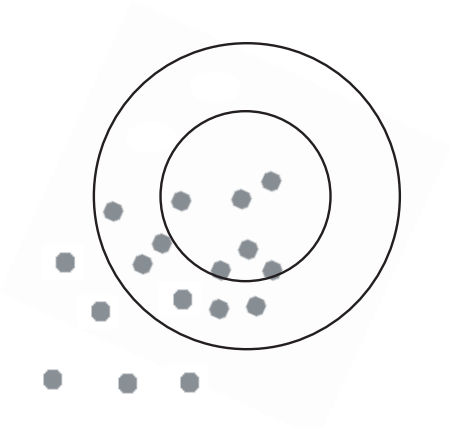

Figure 14: Schooling: Areas of attraction (outer circle) and alignment (inner circle). The gray dots represent organisms.

The Boltzmann Equation

We are interested in finding the form of the probability density function of the system, $\mathcal{P}(\mathbf{X}_1, \mathbf{U}_1, \mathbf{X}_2, \mathbf{U}_2, ..., t)$. The evolution of this quantity is described by

$$\frac{\partial \mathcal{P}}{\partial t} = -\nabla_{\mathbf{x}_i} \cdot (\mathbf{U}_i \mathcal{P}) - \nabla_{\mathbf{u}_i} \cdot (\mathbf{A}_i \mathcal{P}) + \int d^n U' \, T(U - U'|x, U', t) \, \mathcal{P}. \tag{11}$$

If $\mathcal{P}$ is sharply peaked in velocity, the last term on the RHS, which can be thought of as a 'collision' rate, can alternatively be written as

$$\frac{\partial^2}{\delta \mathbf{U}_i \mathbf{U}_j} \left(\frac{\beta_{im} \beta_{jm}}{2} \mathcal{P} \right).$$

If we assume independence of organisms i, which is not true for social behavior, the probabilities are equal for all i, and we can rewrite the evolution as

$$\frac{\partial \mathcal{P}}{\partial t} = -\nabla_{\mathbf{x}} \cdot (\mathbf{U} \mathcal{P}) - \nabla_{\mathbf{u}} \cdot (\mathbf{A} \mathcal{P}) + \frac{1}{2} \nabla^2_{\mathbf{u}} \beta^2 \mathcal{P}. \tag{12}$$

The first term on the RHS represents advection in the x-direction, proportional to the velocity at that point, the second term represents advection towards the x-axis (if $\mathbf{A} \sim -r\mathbf{U}$), and the third term represents diffusion. The first two terms are depicted in Figure 15. As can be seen, organisms will be directed towards the x-axis and parallel to it, resulting formation of a thin filament, which is restrained from reaching zero width by diffusion. In *taxis*, $\mathbf{A}$, the advection towards the x-axis, depends on position $\mathbf{X}$, and in *kinesis*, β, the diffusive term, depends on position.

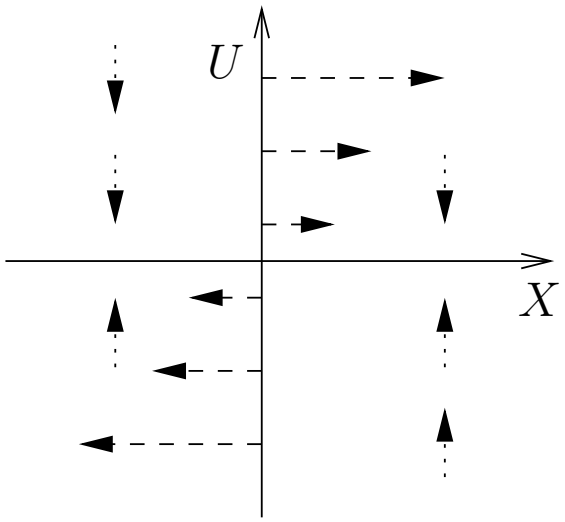

Figure 15: Representation of the directions of the first (dashed) and second (dotted) terms on the RHS of equation (12). In effect, organisms filament along the x-axis, although the diffusive term stops the width from going to zero.

Examples

Example solutions to equation (12), if we define as before $\beta = \beta_0 - \beta_1 C/C_0$ and $\mathbf{A} = -r(\mathbf{U} - \mathbf{u})$, can be seen in Figure 16. Figure 16b) shows that, with diffusion constant in space, i.e. $\beta_1 = 0$, the organisms group in velocity, but not in space. Adding a background flow, $\mathbf{u}$, or diffusion dependent on the cue field $C(x)$, causes grouping in both $|\mathbf{U}|$ and $|\mathbf{X}|$, see Figures 16d) and g).

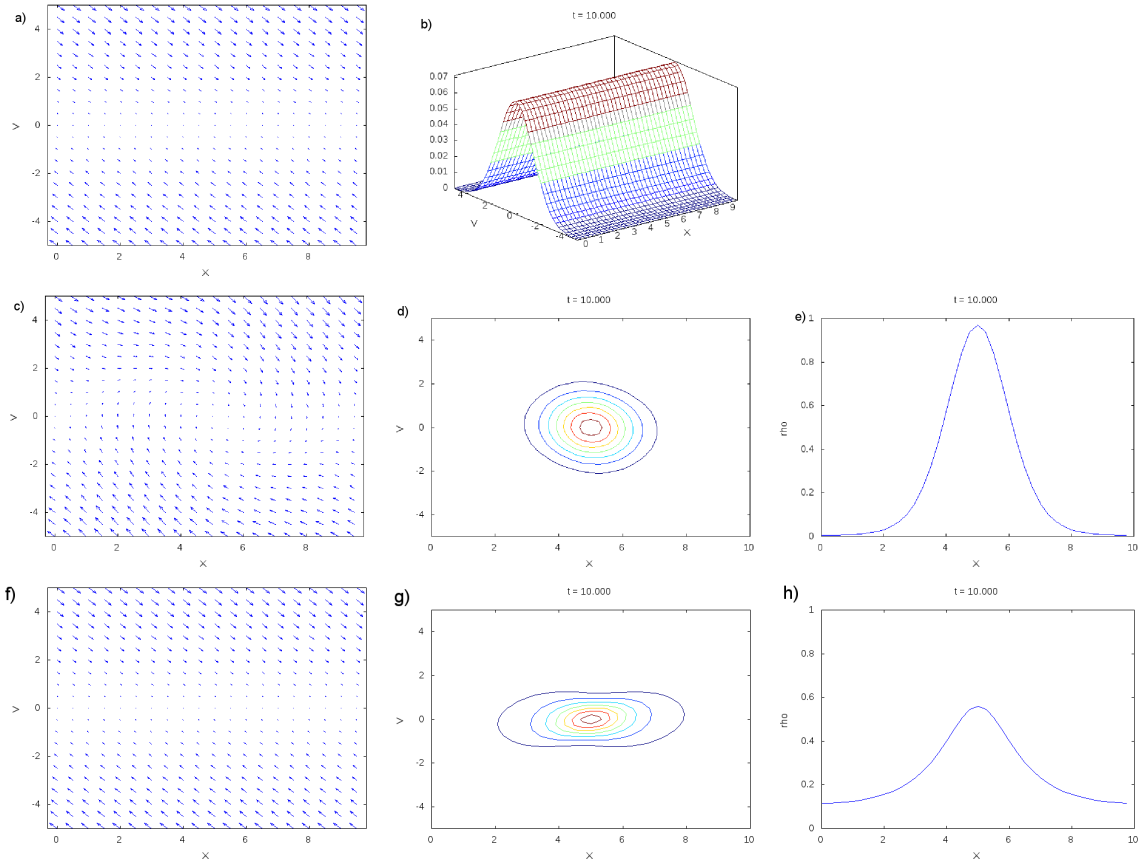

Figure 16: Plots showing the results of solving the Boltzmann equation (12). In a) c) and f), the velocity of the organisms, $\mathbf{U}$, is plotted vs. $|\mathbf{U}|$ and $|\mathbf{X}|$, in b) d) and g), the probability density function $\mathcal{P}$ at large t is plotted vs. $|\mathbf{U}|$ and $|\mathbf{X}|$ and in e) and h), the density of organisms ρ at large t is plotted vs. $|\mathbf{X}|$. Plots a) and b) have $\beta_0 = 2$, $\beta_1 = 0$ and $\mathbf{u} = 0$. Plots c) d) and e) have $\beta_0 = 1$, $\beta_1 = 0$ and $\mathbf{u} = 2$. Plots f) g) and h) have $\beta_0 = 2.7$, $\beta_1 = 2.4$ and $\mathbf{u} = 0$. All quantities have been non-dimensionalised.

Density

Let us define the density, $\rho = \int d\mathbf{U}\mathcal{P}$, and thus the evolution is defined

$$\frac{\partial \rho}{\partial t} = -\nabla_{\mathbf{x}} \int d\mathbf{U}\, \mathbf{U}\mathcal{P} = -\nabla_{\mathbf{x}} \overline{\mathbf{U}} \rho, \tag{13}$$

where the bar indicates a space-mean.

Velocity

This leads to the following expression for the evolution of the quantity $\overline{\rho}\overline{\mathbf{U}_i}$:

$$\frac{\partial(\overline{\rho}\overline{\boldsymbol{U}})}{\partial t} = -\nabla_{\mathbf{x}_j}(\overline{\rho}\overline{\mathbf{U}_i}\,\overline{\mathbf{U}_j} + \overline{\rho}\overline{\mathbf{U}_i'\mathbf{U}_j'}). \tag{14}$$

We can also write $-\nabla_{\mathbf{u}}(A\mathcal{P}) = -\nabla_{\mathbf{u}'}(-r\overline{\mathbf{U}} - r\mathbf{U}')\mathcal{P}$, and then replace these terms back into equation (12). It can be seen that the system is not closed, but if we assume that the three terms in (12) roughly balance, i.e.

$$\overline{\mathbf{U}_i\mathbf{U}_j} \approx \overline{\mathbf{U}}_i\,\overline{\mathbf{U}}_j + \frac{\beta^2}{2r}\partial_{ij},$$

then the system is closed, and $\mathcal{P}$ is now quasi-Gaussian. We can thus derive the closed mass equation

$$\frac{\partial\rho}{\partial t} + \nabla\cdot(\mathbf{U}\overline{\rho}) = 0, \tag{15}$$

and the momentum equation

$$\frac{\partial\overline{\mathbf{U}}_i}{\partial t} + \overline{\mathbf{U}}_j\nabla_j\overline{\mathbf{U}}_i + \frac{1}{\rho}\nabla_i\frac{\beta^2}{2r}\rho = -r(\overline{\mathbf{U}}_i - \mathbf{u}_i - \mathbf{V}_i). \tag{16}$$

Drag Dominated Case

If drag dominates, then we can set the velocity $\overline{\mathbf{U}}$, and so the momentum equation becomes

$$\frac{\partial\rho}{\partial t} + \nabla\cdot(\mathbf{u}\rho + \mathbf{V}\rho) = \nabla\cdot\frac{1}{r}\nabla\frac{\beta^2}{2r}\rho, \tag{17}$$

Taxis vs. Kinesis

Let us re-write equation (17) in terms of diffusivities:

$$\frac{\partial\rho}{\partial t} + \nabla\cdot(\mathbf{u} + \mathbf{V} - \frac{1}{r}\nabla(r\kappa)\rho) = \nabla\cdot\kappa\nabla\rho, \tag{18}$$

where the diffusivity $\kappa = \beta^2/2r^2$ and is spatially varying. The third term on the LHS represents *taxis*, and the fourth *kinesis*. In this form it can be seen that both act similarly on the system, converging velocities to certain regions, either those with smaller velocities (*taxis*) or low diffusivities (*kinesis*). This can also be seen in Figure 17, which shows the initial and final states of organisms experiencing either (*taxis*) or (*kinesis*), as well as the final density states in both cases. However, *kinesis* has similar diffusivities and velocities, i.e. Peclet number is of order 1, while the velocity in *taxis* can be higher.

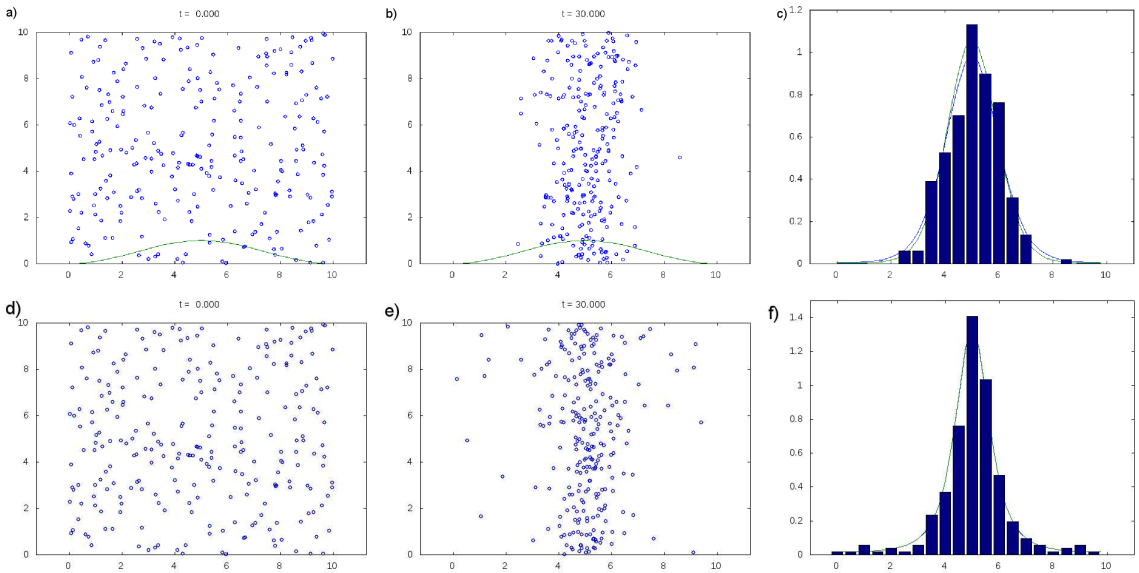

Figure 17: Numerical simulations of the system, assuming either *taxis* in a)-c), i.e. $\mathbf{V} = \alpha \nabla C$ is spatially varying but β is not, or *kinesis* in d)-f), i.e. β is spatially varying but $\mathbf{V}$ is not. The green line in Panels a) and b) shows the distribution of the concentration field C. Panels a), d) and b), e) show the initial and final distributions of organisms. Panels c) and f) show the solutions of the Boltzmann equation (12), [blue line], the density equation (13) [green line] and a histogram of the density in the final snapshot of the simulation. Note that the blue and green lines lie on top of each other in Panel f). These show that, while the biological mechanisms behind them is different, both processes produce similar final density distributions.

Stability with social behavior

In the absence of a background flow, i.e. $\mathbf{u} = 0$, we redefine $\tilde{\mathbf{V}} = \mathbf{V} + \frac{1}{r}\nabla \cdot (r\kappa)$, then

$$\frac{\partial \rho}{\partial t} + \nabla \cdot (\tilde{\mathbf{V}}\rho) = \nabla \cdot \kappa \nabla \rho. \tag{19}$$

The social behavior is specified by making κ a functional of the density, defined in terms of a weighting function w, such that

$$\kappa = K(\int ds\, w(\mathbf{s})\rho(\mathbf{X} + \mathbf{s})),$$

and w takes the form of decreasing with $\mathbf{s}$, which represents the sensing distance of the organism, see Figure 6. If the basic state density is uniform, then κ is constant in space, and we can rewrite ρ and κ as a sum of the means (over-bars) and small perturbations (primes), and so the density equation becomes

$$\frac{\partial \rho'}{\partial t} + \overline{\rho}\nabla \cdot \mathbf{V}' = \nabla \cdot \overline{\kappa}\nabla \rho', \tag{20}$$

where

$$\mathbf{V}' = -\nabla \kappa' = -K'(\overline{\rho})\nabla \int d\mathbf{s}\, w(\mathbf{s})\rho'(\mathbf{X} + \mathbf{s}). \tag{21}$$

Taking a Fourier transform of this equation, we can find an expression for the growth in density perturbations:

$$\frac{\partial}{\partial t}\hat{\rho}' = [\overline{\rho}K'(\overline{\rho})k^2\hat{w}(k) - \overline{\kappa}k^2]\hat{\rho}. \tag{22}$$

If the bracketed term is greater than zero, the system experiences positive growth see Figure 18, which shows the relationship between growth rate and wave number k. In fact, the system experiences explosive (faster than exponential) growth, with the amplitude going as

$$\frac{\partial A}{\partial t} = \sigma(k)A + \mathcal{N}A^3,$$

where $N > 0$.

Evolution of Social Behavior

I: Inheritance of Traits

As before, we define the velocity $\mathbf{V}$ as the gradient of a scalar, i.e. $\mathbf{V} = \nabla\phi$, see [7], where

$$\phi = w_0 \int d\mathbf{s}\, w(\mathbf{s})Z(\mathbf{X} + \mathbf{s}), \quad \int d\mathbf{s}\, w(\mathbf{s}) = 1. \tag{23}$$

In this case, the weighting function $w(\mathbf{s})$ takes the form depicted in Figure 19 with repulsion at short distances.

We define three different genetic types, or alleles, of the heterotroph Z (which preys on P), each with two genes with two possible genetic traits, 0 or 1: Z_{00}, Z_{01}, Z_{11}. Z_{00} and Z_{11}

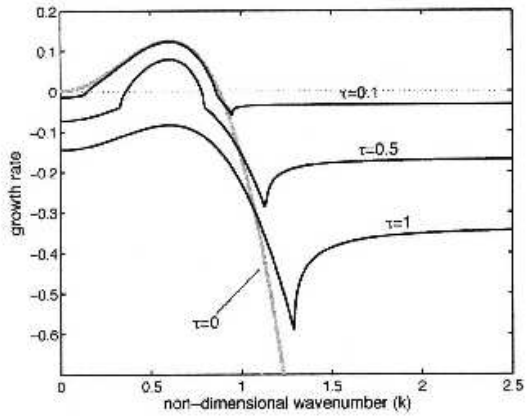

Figure 18: Figure from [7], showing "the linear growth rate of small perturbations around the equilibrium biomass versus the wave number of the perturbations, ... for different values of τ", $\propto 1/\kappa$, a diffusion time scale. "In a uniform distribution of particles, random variations will spontaneously lead to the formation of patches, if there is positive growth somewhere along the wave number spectrum. The gray line shows the case where particle motion is decoupled from biological activities. ... When the diffusion rate is fast compared to growth ($\tau << 1$), population dynamics have a negligible impact on the linear growth rate of perturbations in the region of instability (positive growth). As biological processes become faster, their effect ... [is to] stabilize the equilibrium solution; the growth rate is negative for all wave numbers when $\tau \approx 1$".

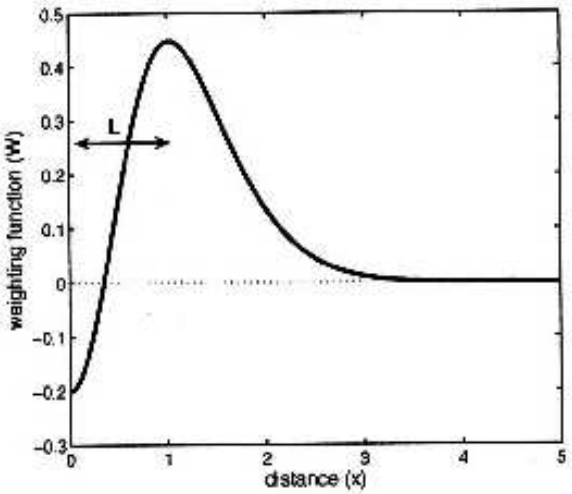

Figure 19: Figure from [7], showing the weighting function, $w(x)$, of organisms as function of their distance from neighbors located at $x = 0$, as used in equation (23). "$w(x) = exp(-x^2/2) - exp(-2x^2)$. Distances are expressed in units of L, the characteristic perception length scale. The sensing radius has an approximate value of $2L$. ... Positive weighting indicates attraction to neighbors. Repulsion at short distance prevents over-crowding."

are recessive, and only Z_{11} exhibits grouping behavior, i.e. $\mathbf{V}_{00} = \mathbf{V}_{01} = 0$, $\mathbf{V}_{11} \neq 0$. The population of each type evolves as follows:

$$\frac{\partial}{\partial t} Z_{\alpha\beta} = ag \frac{P}{P + P_h} \frac{f_{\alpha\beta}}{Z + c} - dZ_{\alpha\beta} - \nabla \cdot (\mathbf{V}_{\alpha\beta} - \kappa\nabla) Z_{\alpha\beta} + M_{\alpha\beta}, \tag{24}$$

where $0 \leq a \leq 1$ is the conversion efficiency of P into biomass by Z, $0 \leq g \leq 1$ is a grazing rate, d is the death rate, P is the population of prey and $f_{\alpha\beta}$ is the inheritance fraction of the population $Z_{\alpha\beta}$. P_h is the half-saturation density, which provides a limitation to the amount of prey that can be eaten at large P, i.e. Z depends linearly on P until the capacity of Z to eat P becomes reached. The c term represent the "Allee" effect [1]: as the density Z is small, encounters between male and female organisms are rare and depend quadratically on density, whereas for large Z virtually all females have mated and reproduction depends linearly on the population gets large, virtually all females have mated. From a Mendelian table of inheritance[4] we can define the fractions $f_{\alpha\beta}$ as:

$$\begin{aligned}
f_{00} &= Z_{00}^2 + Z_{00}Z_{01} + \frac{1}{4}Z_{01}^2, \\
f_{01} &= Z_{00}Z_{01} + 2Z_{00}Z_{11} + \frac{1}{2}Z_{01}^2 + Z_{01}Z_{11}, \\
f_{11} &= Z_{11}^2 + Z_{11}Z_{01} + \frac{1}{4}Z_{01}^2, \\
Z^2 &= f_{00} + f_{01} + f_{11} = (Z_{00} + Z_{01} + Z_{11})^2,
\end{aligned}$$

where this implies that, for example, a new generation of Z_{00} is produced by all interactions between two Z_{00}, half of the interactions between Z_{00} and Z_{01}, and 1 in 4 of interactions between two Z_{01}.

We also include a mutation term, $M_{\alpha\beta}$, which allows for the possibility of a population reforming if it dies out completely:

$$\begin{aligned}
M_{00} &= -\mu Z_{00} + \frac{1}{2}\mu Z_{01}, \\
M_{00} &= -\mu Z_{01} + \mu Z_{00} + \mu Z_{11}, \\
M_{11} &= -\mu Z_{11} + \frac{1}{2}\mu Z_{01},
\end{aligned}$$

where μ is the fractional rate of mutation. The prey, P evolve as follows;

$$\frac{\partial P}{\partial t} = bP\left(1 - \frac{P}{P_c}\right) - g\frac{P}{P + P_h}\frac{Z^2}{Z + c} + \nabla\kappa\nabla P, \tag{25}$$

where b is the growth rate, P_c is the half-saturation density, and all other quantities are as before.

Examples

There are specific conditions under which the grouping type, 11, can win out with respect to the other two types. If the grouping strength is not too high and/or the diffusivity is not too low, then it can cause the extinction of the other two species, due to the reproduction

advantages of grouping, see Figures 20a) and b). However, if the diffusivity is too low to bring the grouping type sufficient prey, then the other two types will dominate, while the grouping type will die out until the groups are sufficiently small to survive, see Figures 20c) and d). If the grouping species, 11, is introduced at low values to the other two types, then it will slowly take over until it reaches a critical fraction, f_c, at which the other two species become extinct and the grouping type wins, see Figure 21.

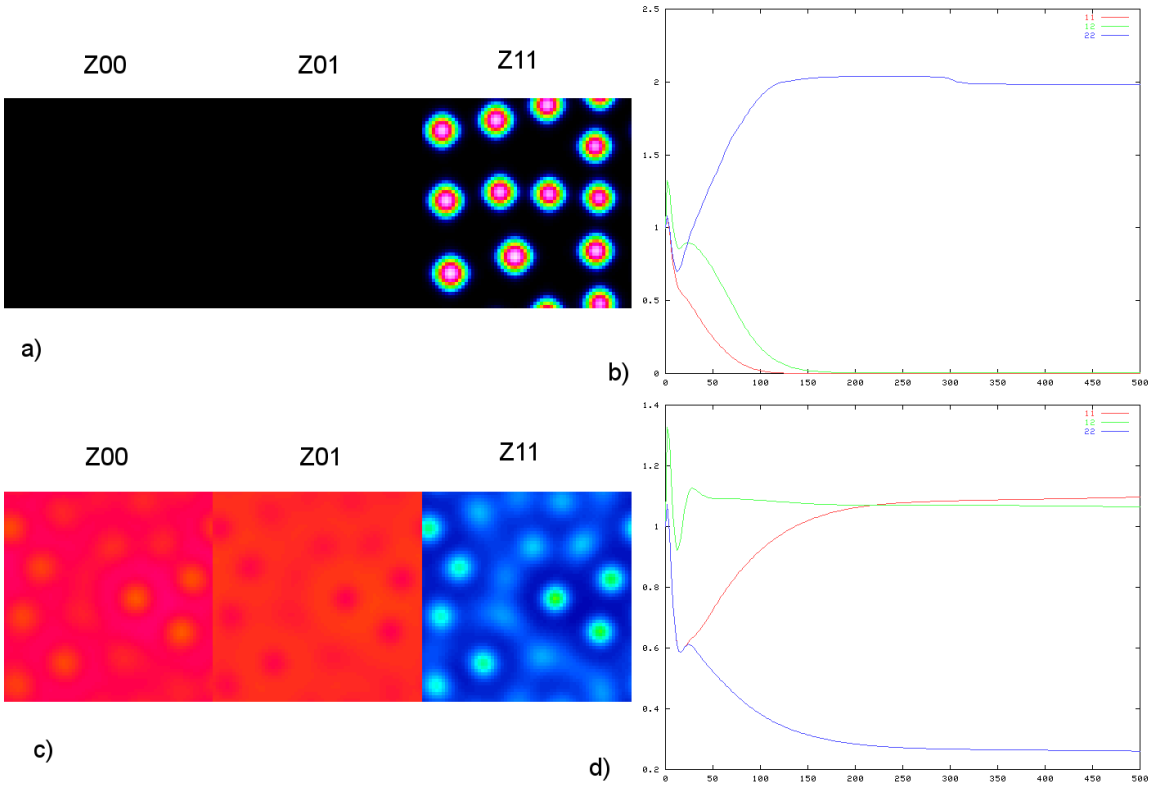

Figure 20: Final state population distributions $Z_{\alpha\beta}$ from numerical simulations (a) and c)) shown next to the fractional populations $f_{\alpha\beta}$ over time (b) and d)). In a) and b), the species Z_{11} causes the other two to die out, due to the advantages of grouping for reproduction. However, if the diffusivity is low, as in c) and d), then the disadvantages of grouping, i.e. the fast depletion of prey, mean that Z_{00} and Z_{01} do much better than Z_{11}, which doesn't completely die out.

If we subject the system to background stirring motion, such as Ray Pierrehumbert's exact sin/sin stirring[5], see Figure 22(i), then we can test whether grouping is still advantageous or not, see Figures 22(ii)-(v). It can be seen that, at low grouping parameters and low stirring, the grouping type dies out, but at large grouping parameters and large stirring, the grouping type wins. In other regimes, both types survive.

Thus, it is not only the biological but the dynamical features which can determine how a particular species will fare.

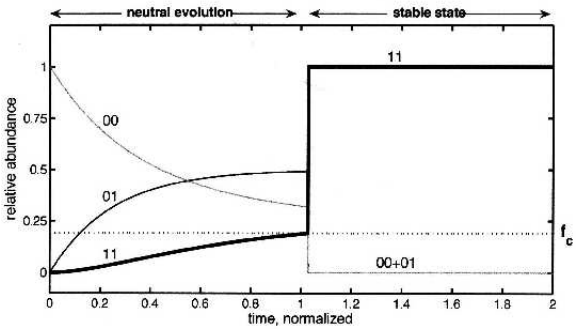

Figure 21: Frequency of $Z_{\alpha\beta}$ versus time, showing the invasion of a non-grouping population, Z_{00}, by the grouping type, Z_{11}, taken from [7]. "Time is normalized by the mutation timescale ... The new allele, introduced at low frequency at $t = 0$ does not affect fitness until the frequency of grouping organisms (type 11) reaches f_c, at which part it starts to aggregate. ... In this case, social behavior is a successful strategy: the grouping type wins the competitions and the other types become extinct. The ecosystem is then stable with respect to mutations in the two-allele model."

II: Grouping Parameter

Examples of how diffusion and grouping affect the dynamics when limit cycles may be present (through setting the value of c in (24)), can be seen in Figure 23.

To find optimal parameters, we let populations with different grouping strengths compete, and note whether their populations grow or decay. The effect of the half saturation ratios, P_h and c in equation (24), on the optimal grouping strength can be seen in Figure 24.

III: Schooling

As before, we represent schooling as velocity alignment with neighbors and attraction (except very nearby). We add a food supply, confined to the mixed layer at the top of the ocean, with variability produced by upwelling which brings further nutrients. As the mixed layer is by definition assumed well-mixed, downwelling does not change the concentration of nutrients. We specify a streamfunction, ψ, and a vertical velocity, w, that depend on the depth of the thermocline, h:

$$\psi = \frac{g'}{f}h, \quad w = -\frac{\partial h}{\partial t}, \tag{26}$$

where g' is the modified gravitational acceleration and f is the planetary vorticity. We can then derive the evolution of the nutrient, N:

$$\frac{\partial N}{\partial t} = \frac{w(w>0)}{H}(N_{deep} - N) - \mu NP + \nabla.\kappa_{fluid}\nabla N, \tag{27}$$

where H is the average depth of the thermocline, N_{deep} is the nutrient value at depth, and P is the population of the autotroph, e.g. phytoplankton. Example biomass distributions from numerical simulations can be seen in Figure 25.

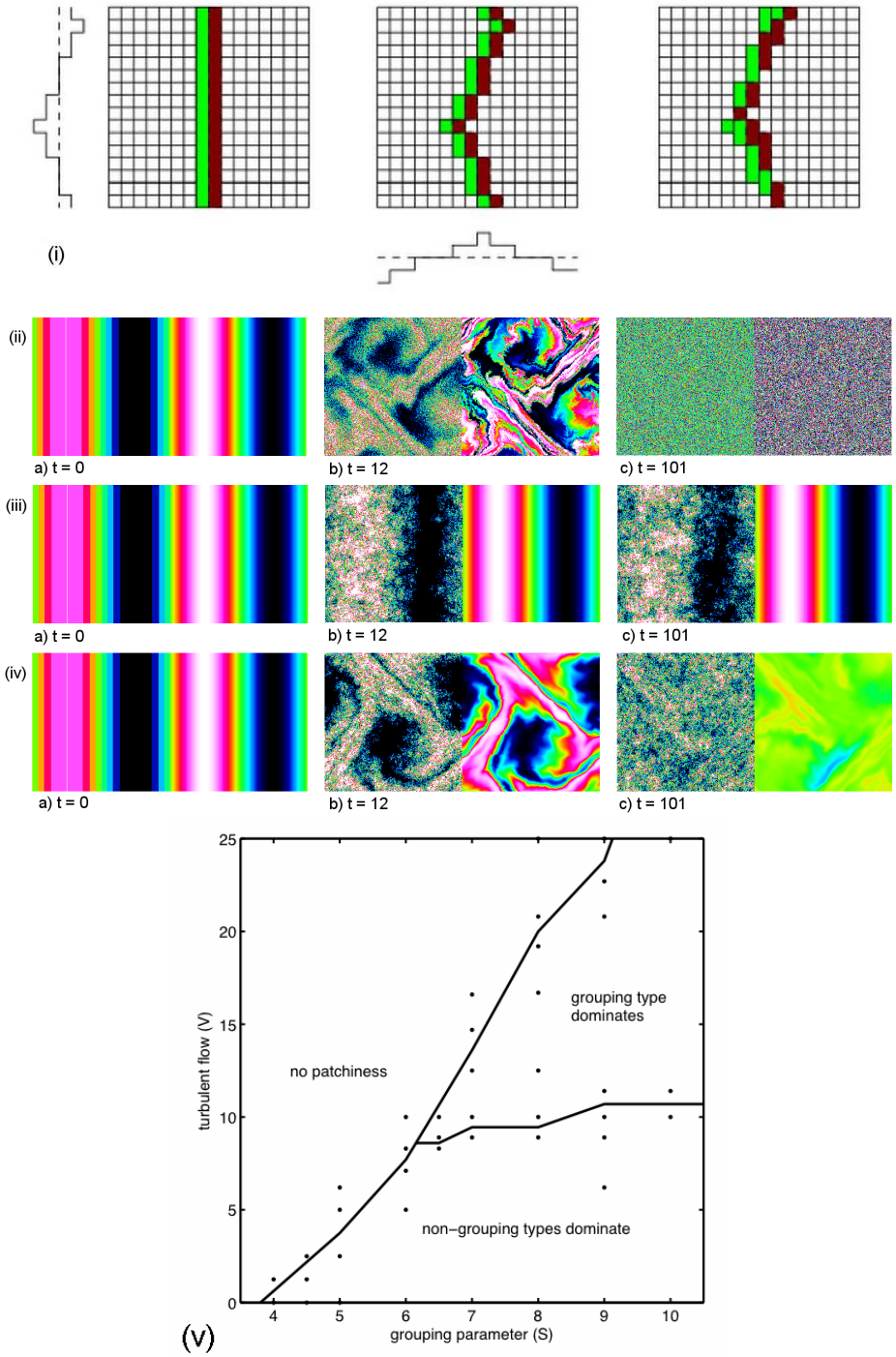

Figure 22: (i) depicts the form of the Pierrehumberts exact sin/sin stirring. $(ii) - (iv)$ show snapshots from numerical simulations of Z_{11} (left panels) and a passive tracer (right panels); (ii) and (iii) have no diffusion, i.e. $\kappa = 0$, (ii) and (iv) are subject to a medium rate of stirring, and (iii) is not subject to any stirring. (iv) shows that, while diffusion eventually completely removes any gradients in the tracer, Z_{11} still remains grouped. (v) shows a summary of the conditions where grouping and non-grouping Z survive, from [7].

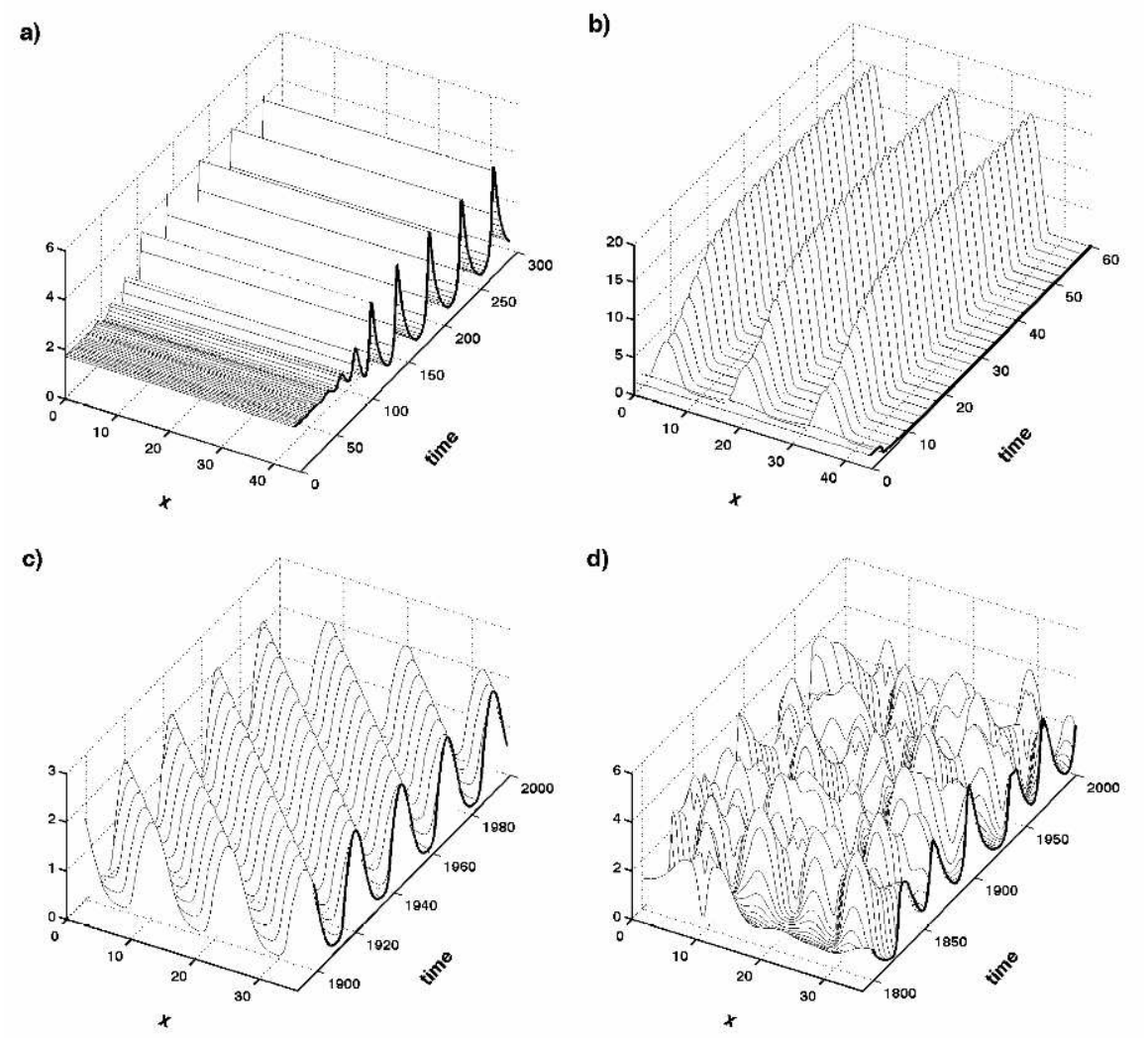

Figure 23: Numerical simulations of predator biomass, Z, distribution in time and space, from [6]. "Thin black contours show the instantaneous spatial distribution, at fixed intervals in time. Thick black curve shows the time series of biomass at a fixed location. a) Without aggregation behavior" ($w_0 = 0$), "the predator-prey system reaches a limit cycle after a period of transients; the simulation shown here is initialized near the unstable coexistence fixed point. b) With social behavior" ($w_0 = 2$), "and fast diffusion, patches form spontaneously and the system loses its oscillatory behavior. c) With social behavior" ($w_0 = 15$), "and slow diffusion, the system supports a regular wave traveling through the domain; transients are not shown. d) With social behavior" ($w_0 = 5$), "and slow diffusion, the density field can appear chaotic."

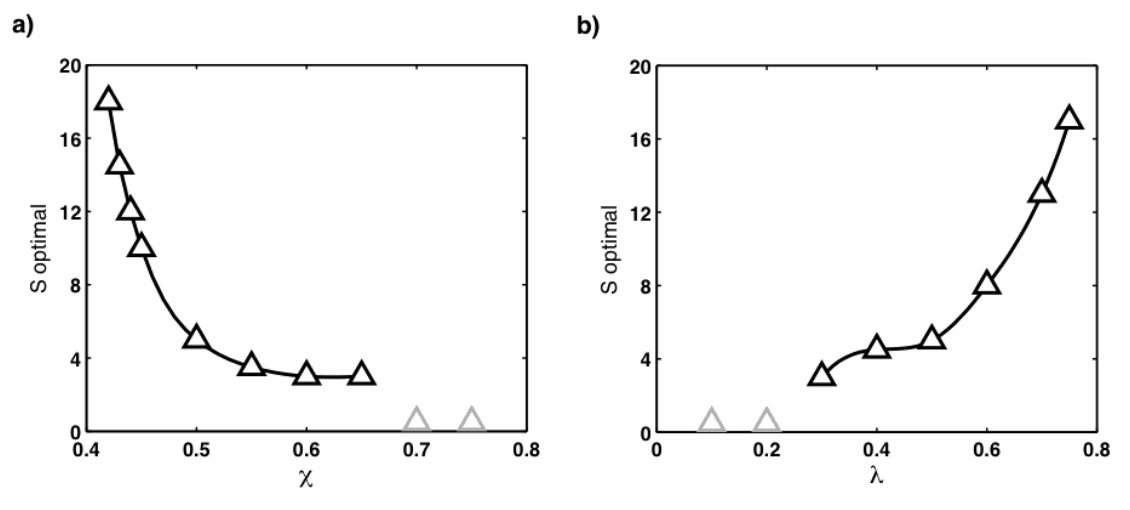

Figure 24: Optimal strategy vs P_h and c, from [6]. χ is non-dimensionalised P_h, λ is non-dimensionalised c, and S is our w_0. "Black symbols indicate optimal parameter values of $[w_0]$ from numerical simulations of the competition model, solid line is the spline interpolation. Gray symbols indicate that social behavior is not a successful strategy, in which case non-grouping types ... are the best competitors."

We model foraging by assuming that the turning rate of an organism is dependent on the difference between past feeding, ξ compared to current food values. Here we consider the turning rate $\delta\theta$ of a heterotroph, Z, in terms of the population of its prey, P. The memory of food evolves as follows:

$$\frac{\partial \xi_i}{\partial t} = \frac{P(\mathbf{X}_i)}{P(\mathbf{X}_i) + P_h} - \frac{\xi_i}{\tau}, \tag{28}$$

where τ is the memory period of the heterotroph. Then we model the turning as

$$\delta\theta = 1 + \tanh(\alpha(\xi_i - P(\mathbf{X}_i)), \tag{29}$$

where α is a constant. Figures 26 and 27 show how the success of the foraging Z depends on how fast they swim. Foragers that are too speedy over-shoot the largest concentrations of prey; slow foragers, however, don't find the prey for a long time. Figure 28 shows how successful schooling is for foragers in various levels of turbulence and resources. It can be seen that, for low levels of resources there is no clear advantage to schooling, and it can actually be a disadvantage at low levels of α, the ratio of alignment to attraction, as defined in equation (29). However, in cases with medium or high resources, there are values of α that provide a clear advantage.

Aggregation

Observations of Antarctic krill swarms can be seen in Figure 29. Generally, during the day there tends to be many small swarms near the surface, and at night there tend to be a

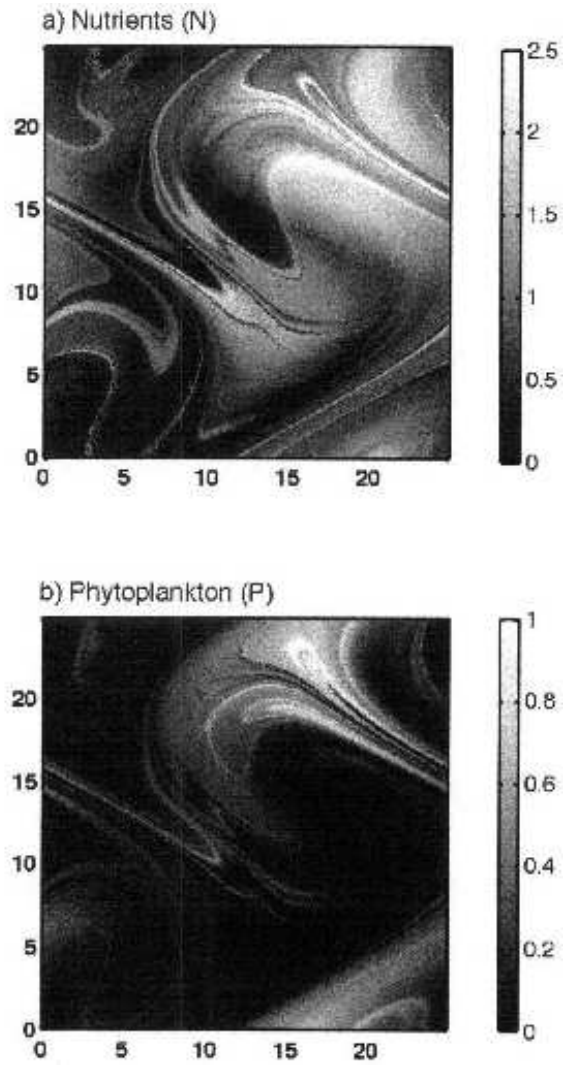

Figure 25: Figure from [6], showing results from numerical simulations with schooling and turbulent advection. a) biomass of nutrients N, b) biomass of phytoplankton P. "Lighter shades of gray indicate larger values. The two fields tend to be anti-correlated."

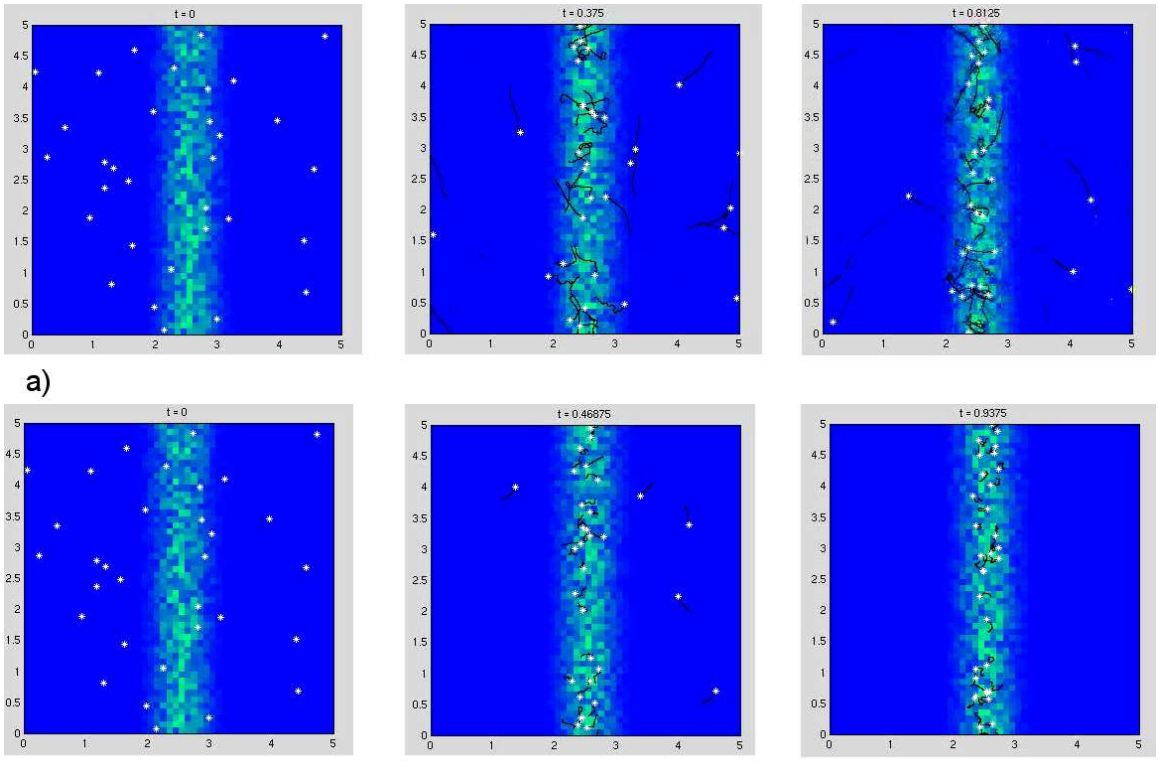

Figure 26: Figures showing numerical simulations of foraging Z with a) fast swimming speeds and b) slow speeds at various non-dimensionalised times. The white dots represent the individual Z, the black tails represent the organism's grazing memory and the color scale represents the concentration of prey P. It can be seen that the fast swimmers overshoot and never all end up concentrated on the prey, whereas the slow swimmers quickly group over the high concentration of prey.

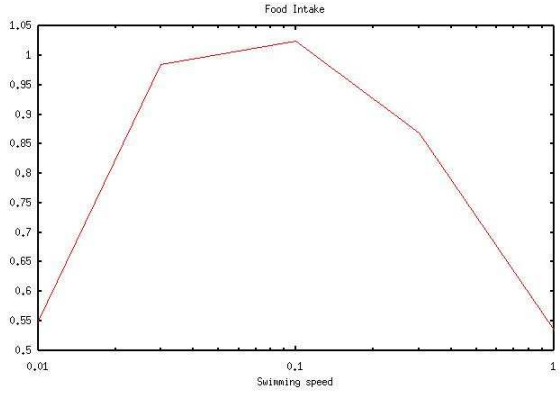

Figure 27: Figure summarizing the (non-dimensionalised) food intake of foraging Z with a specific swimming speed from numerical simulations. Clearly there is an ideal swimming speed at which the swimmers find the food within a reasonable time but do not overshoot the highest concentration by swimming too fast.

few large swarms at depths (∼250m). Different types of aggregation can be classified using a measure of polarization: the degree to which the grouping is swarm-like or school-like. Figure 30 shows results from numerical simulations, with the degree of polarization plotted against the degree of alignment, α, and the swimming velocity, V. Five specific grouping phases are identified and examples shown of each.

Conclusion

It can be seen that a wide range of grouping structures in organisms can be simply modelled. We have seen that in turbulent environments it is sometimes advantageous to school or group, depending on the properties of the organisms themselves as well as how the environment affects their supply of food. In general, it seems that there is the need for a certain amount of resource availability to make it advantageous for foraging predators to school.

References

[1] W. C. Allee, *Principles of animal ecology,*, Philadelphia, Saunders Co., 1949.

[2] C. W. Gardiner, *Handbook of Stochastic Methods for Physics, Chemistry and the Natural Sciences*, Springer, 3rd ed., 2003.

[3] G. Lawson, *Distribution, patchiness, and behaviour of antarcti zooplankton, assessed using multi-frequency acoustic techniques.*, PhD thesis, MIT-WHOI Joint Program in Oceanography, 2006.

[4] G. Mendel, *Versuche ber pflanzen-hybriden*, Verh. Naturforsch. Ver. Brnn, 4 (1866), pp. 3–47.

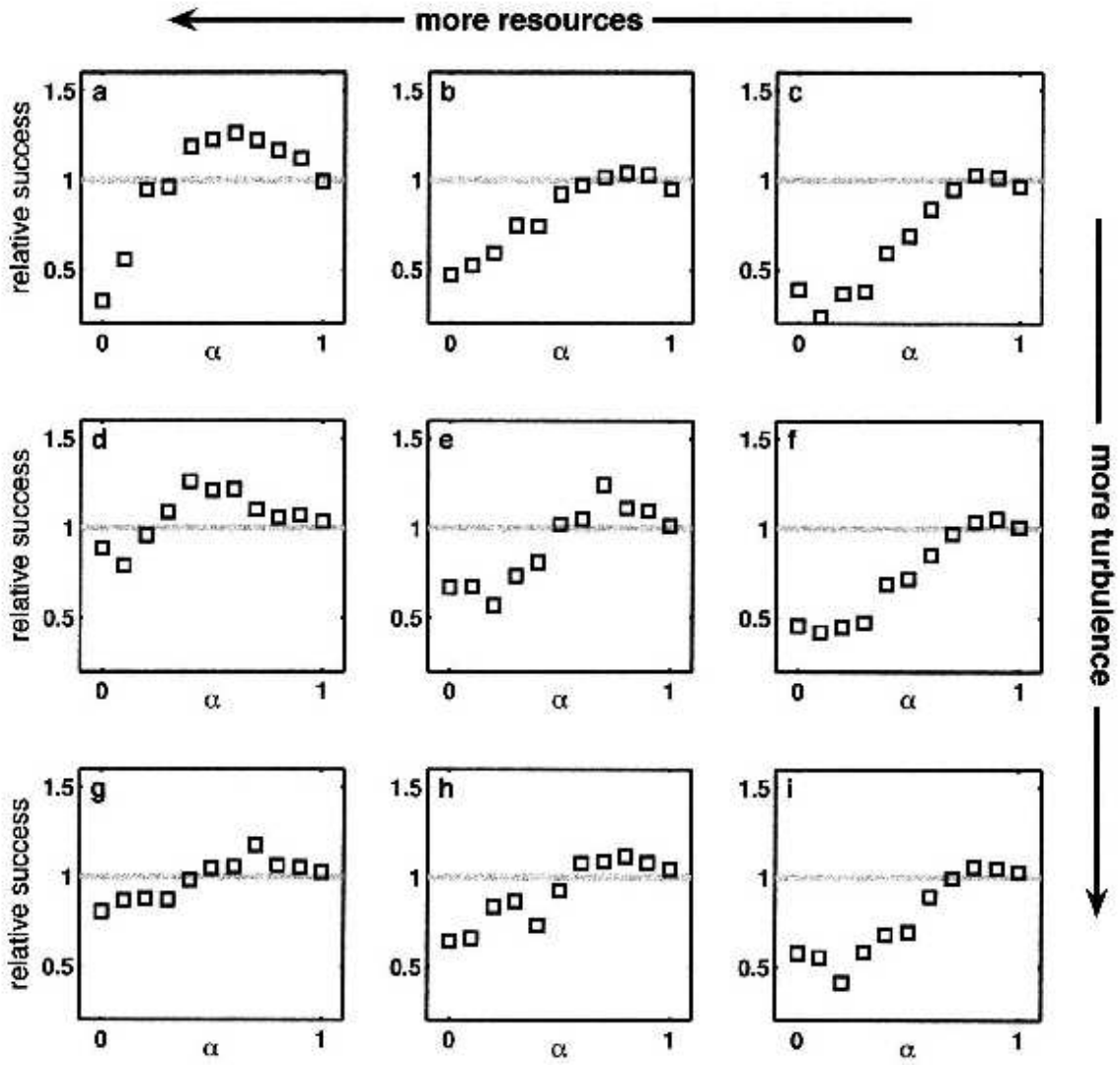

Figure 28: The foraging success of schooling Z, taken from [6], "normalized by the success of random walkers under the same conditions. In each panel, the relative success ... is shown for different strategies (α, the ratio of alignment to attraction", see equation (29) "varying between 0 and 1). Each column corresponds to a different level of resource availability; each row has different flow characteristics." In the low resource panels, there is no advantage to schooling, and in fact it can be a disadvantage at low values of α. However, with medium to high resources, there are values of α that provide a clear advantage.

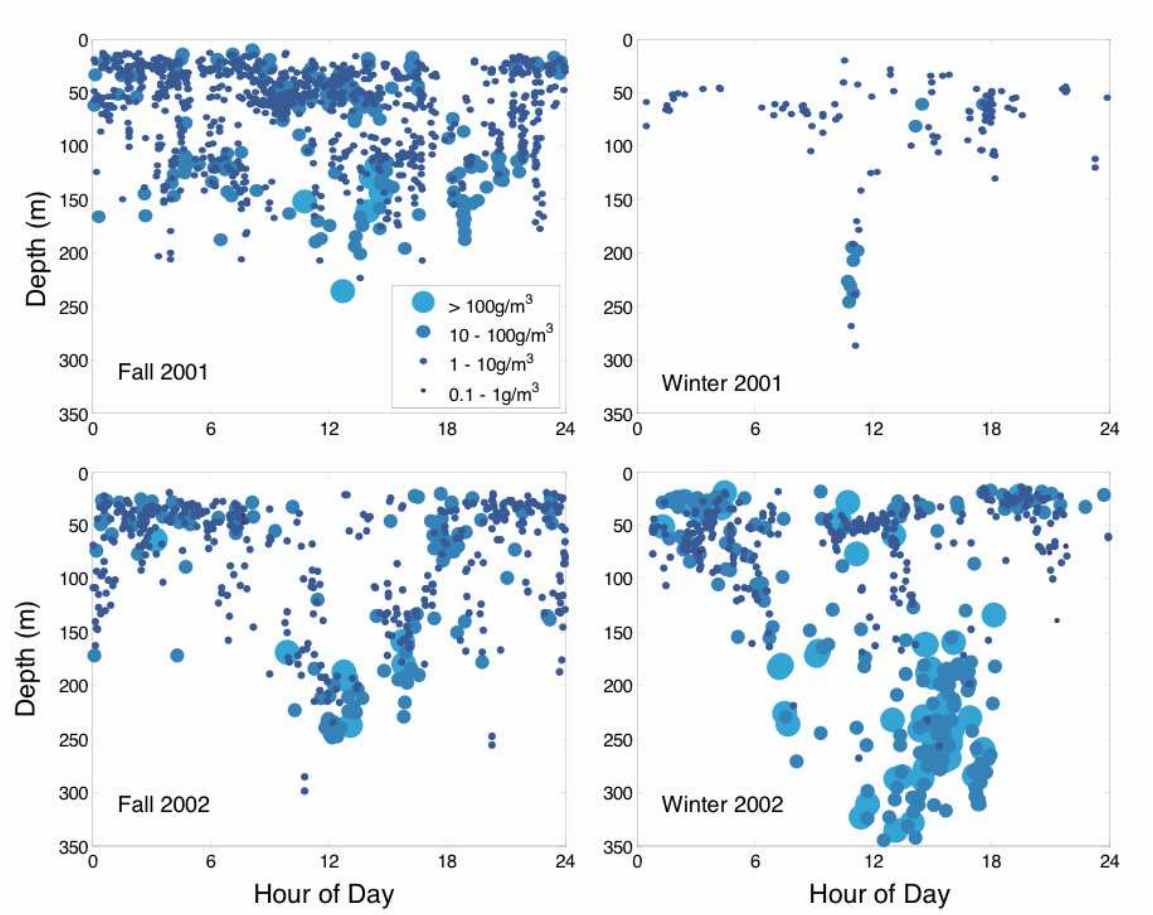

Figure 29: Observations of Antarctic krill from acoustic measurements [3]. Points represent aggregations, which are plotted as a function of the time of day of observation (x-axis) and mean depth (y-axis). The size and color represent the mean density. The general trend shows a few patches of large density at depth at night and many patches of small density near the surface during the day.

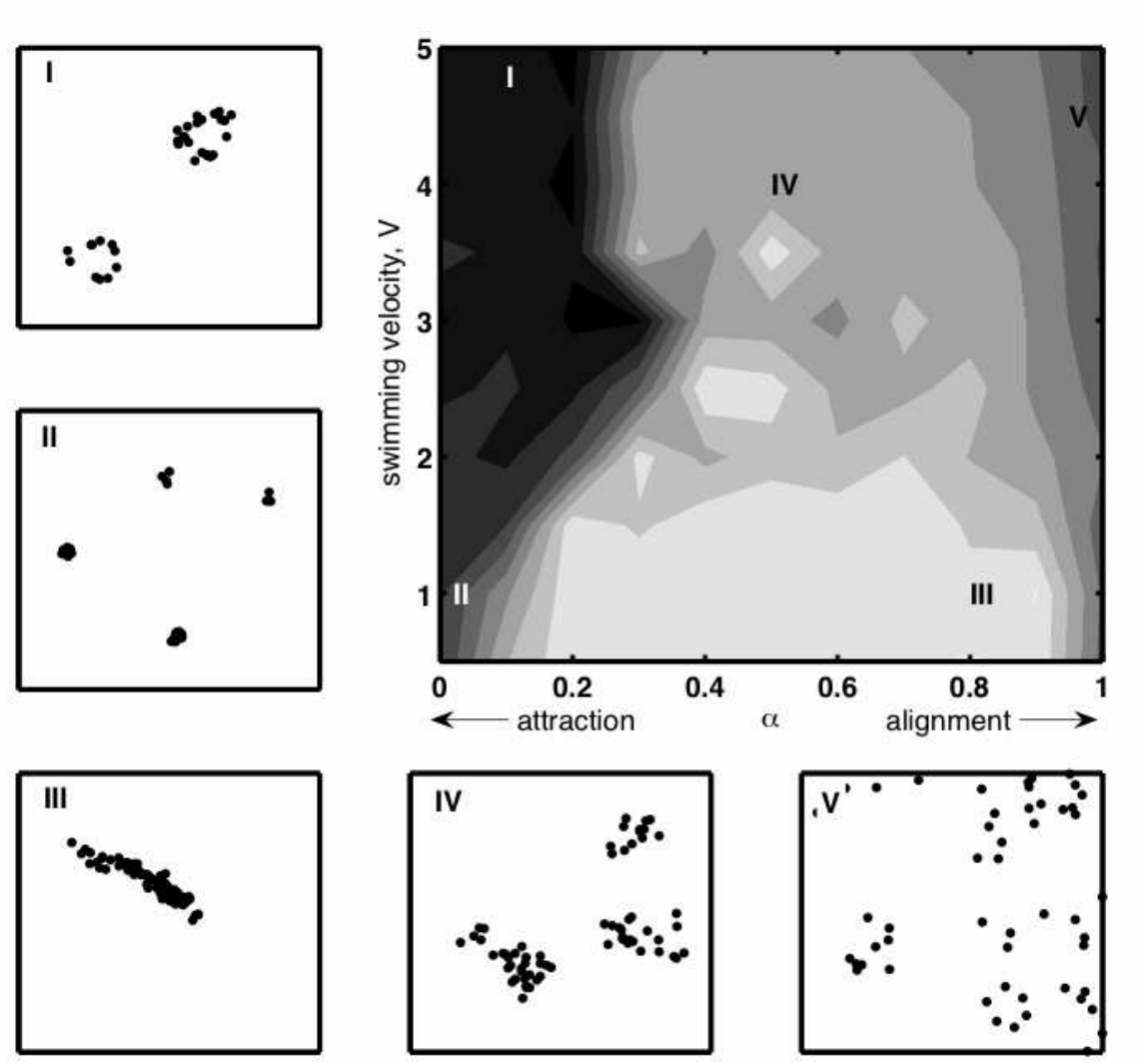

Figure 30: Simulations results from [6]. The gray shading indicates the degree of polarization; high vales (light gray) represents schooled groups, low values (black) represent swarming groups. This is plotted against α, degree of alignment, and V, swimming velocity. Labels I-V indicate distinct phases: I milling; II swarms; III large schools; IV small schools; V transient alignment.

[5] R. Pierrehumbert, *Tracer Microstructure in the Large-Eddy Dominated Regime*, Chaos Solitons & Fractals, 4 (1994), pp. 1091–1110.

[6] A. Verdy, *Dynamics of marine zooplankton: social behavior, ecological interactions, and physically-induced variability*, PhD thesis, MIT-WHOI Joint Program in Oceanography, 2007.

[7] A. Verdy and G. Flierl, *Evolution and social behavior in krill*, Deep Sea Research Part II: Topical Studies in Oceanography, 55 (2008), pp. 472 – 484. Dynamics of Plankton, Krill, and Predators in Relation to Environmental Features of the Western Antarctic Peninsula and Related Areas: SO GLOBEC Part II.